MM Science Journal | www.mmscience.eu
ISSN 1803-1269 (Print) | ISSN 1805-0476 (On-line)
Special Issue | HSM 2025
18th International Conference on High Speed Machining
October 15-16, 2025, Metz, France
DOI: 10.17973/MMSJ.2025_12_2025156

HSM2025-44829

INDIRECT TOOLTIP FREQUENCY RESPONSE FUNCTION MEASUREMENT: AN APPLICATION OF SURFACE LOCATION ERROR

L. Morelli[1]*, N. Grossi[1], G. Campatelli[1], A. Scippa[1]
[1]Department of Industrial Engineering, University of Firenze, Via di Santa Marta 3, 50139, Firenze, Italy
*Corresponding author; e-mail: lorenzo.morelli@unifi.it

Abstract
Milling is a well-established manufacturing process thanks to its accuracy and surface finishing, yet tool vibrations limit these qualities. At the core of many approaches dealing with vibrations the tool-tip frequency response function (FRF) is found allowing the computation of the appropriate cutting conditions for accuracy and stability. The evaluation of the tooltip FRF is often based on experimental modal tests which require additional sensors to be mounted on the machine tool as well as devices to excite the tool. However, the reliability of these methods is strictly related to the test setup and the expertise of the operator performing the measurement. This paper presents a methodology to evaluate the tooltip FRF starting from the surface location error (SLE) without requiring additional sensors or experienced operators. The method is based on a frequency domain cutting force model coupled with the SLE measured at different spindle speeds using on-machine measuring probe. The methodology was experimentally tested to check its effectiveness and limitations.

Keywords:
End Milling, Vibration, Surface location error

1 INTRODUCTION

Milling is one of the most common processes adopted in the finishing of mechanical components thanks to its accuracy and surface finishing, yet when the tool flexibility is relevant, as it happens in certain operations, the rise of vibrations may negatively impact on the cutting process causing out of tolerance components and poor finishing [Mann 2008]. To overcome these limitations, many methods are available in literature, from predictive methods to be used before the cut to damping techniques to be used during the cut [Munoa 2016]. Among predictive methods tool deflection estimation [Llanos 2023] and Stability lobe Diagrams (SLD) [Niu 2021] are widely used to evaluate the effect of vibrations on surface errors and cutting stability respectively with the aim of preselecting suitable cutting parameters. On the other hand, damping techniques adopt both passive and active devices to increase damping of the system so that on the occurrence of vibrations their impact is reduced [Kleinwort 2016, Kolluru 2013]. At the base of these methods lies the tooltip Frequency Response Function (FRF) which identifies how the tooltip responds in terms of displacement to an input force at different frequencies. In detail, for a reliable system able to reduce vibrations, it is important to have an accurate experimental estimation of the tooltip FRF. However, measuring the tooltip FRF is complex due to the uncertainties and limitations associated with the current techniques.

Typically, the tooltip FRF is obtained with Experimental Modal Analysis (EMA) using different sensors to excite the tooltip and capture its response. One of the common methods employed in EMA is the Impact Hammer Testing where an instrumented hammer excites the tooltip, and an accelerometer measures its response. For the ease of use this method is widely spread, but its reliability is affected by poor repeatability which heavily depends on the operator's skill. Additionally, impact testing must be conducted while the machine tool is idle, failing to account for operational aspects such as spindle speed which may affect the tooling system behavior [Iglesias 2022].

To overcome this gap, alternative methods for identifying tooltip FRF under operational conditions have been the subject of many research activities. For example, Wiederkehr et al. [Wiederkehr 2020] introduced a method for evaluating tooltip FRF in micro-milling by hitting a rotating tool with microspheres. Conversely, Zaghbani et al. [Zaghbani and Songmene 2009] employed Operational Modal Analysis (OMA) to estimate tooltip FRF exploiting only accelerometer signals collected during cutting operations; Even if this approach reflects actual operational conditions, it neglects the excitation source leading to limitations in the definition of FRF parameters. To overcome this issue, Aguirre et al. [Aguirre 2014] used cutting force harmonics as excitation input to estimate fixture FRF though a dynamometric tool holder.

Generally, existing methods for identifying tooltip FRF often require additional sensors to be installed on the machine tool. Depending on the precision accuracy required, these methods can be both costly and time-consuming. However, Budak et al. [Tunc and Budak 2013] proposed an analytical inverse method that identifies certain FRF parameters (such as damping ratios) directly from chatter tests without additional sensors. This approach accounts for actual

operaional conditions, but it is limited to simple operations due to the constraints of the analytical model used.

In this context, this paper explores an inverse analytical method to estimate the tooltip FRF using only a measuring probe, which is commonly available on modern machine tools. Specifically, the method focuses on peripheral milling, which exhibits a distinct characteristic: the surface error is not uniform but varies along the tool axis. This error, known as Surface Location Error (SLE), depends on cutting conditions and can be predicted using the analytical model introduced by Schmitz et al. [Schmitz and Mann, 2006].

The proposed method is based on measured SLEs obtained from cutting tests coupled with a frequency-domain cutting force model to estimate tooltip FRF. The approach has been experimentally validated to assess its effectiveness. Although its applicability is limited to peripheral milling and simple operations according to the analytical model considered, its simplicity and ease of use make it a compelling alternative.

2 PROPOSED APPROACH

The aim of the proposed approach is estimating the tooltip FRF in peripheral milling using measured SLEs. In particular, the tooltip FRF, which this work is focused on, is the direct tooltip FRF in the cross-feed direction (*y*) according to the mechanism of surface generation in peripheral milling where surface errors depend for the most by the tool vibration orthogonal to the surface [Morelli 2021].

In this context, referring to *Fig. 1*, due to the tool helix SLE is not constant along the axial depth of cut (a_p), but it features a particular profile which changes with tool geometry, cutting parameters and cutting strategy (i.e., Down-milling or Up-milling).

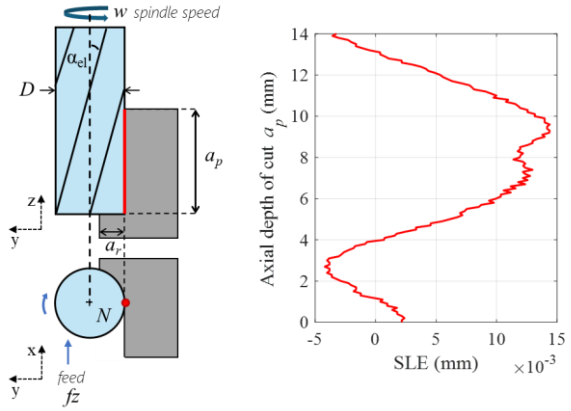

Fig. 1: Peripheral milling process and SLE.

These aspects affect the time interval in which SLE is created according to the following equations:

$$\frac{\phi_{out}}{2\pi w} \leq t_s \leq \frac{\phi_{out}+\alpha_{sw}}{2\pi w} \quad \text{Down-milling;} \tag{1}$$

$$\frac{\phi_{in}}{2\pi w} \leq t_s \leq \frac{\phi_{in}+\alpha_{sw}}{2\pi w} \quad \text{Up-milling;} \tag{2}$$

$$\alpha_{sw} = k_b a_p, \tag{3}$$

$$k_b = 2\tan(\alpha_{el})/D, \tag{4}$$

where t_s is the time instant in which the machined surface is generated, ϕ_{out} and ϕ_{in} are the tool exit and entry angles respectively, α_{sw} is the axial engagement angle, w is the spindle speed expressed in rpm, and D is the tool diameter.

To predict SLE including its shape, the closed form solution presented by Schmitz et al. [Schmitz and Mann 2006] represent a reference model thanks to its simplicity and effectiveness. In detail, SLE can be summarized with a simple equation in the frequency domain:

$$Y(\omega) = H_{yy}(\omega) * F_y(\omega); \tag{5}$$

where ω represents the frequency variable of this domain, $Y(\omega)$ is the tooltip displacement spectrum along the y direction, $F_y(\omega)$ is the cutting force spectrum in the same direction and $H_{yy}(\omega)$ is the corresponding direct tooltip FRF. Translating $Y(\omega)$ of Eq.5 from the frequency domain to the time domain SLE is found as:

$$SLE = y(t_s); \tag{6}$$

where $y(t)$ is the tooltip displacement in the cross-feed direction in time domain and SLE is the tooltip displacement evaluated in the time interval t_s in which machined surface is generated.

In this work the analytical model proposed by Schmitz et al. is inverted and used to compute the tooltip FRF $H_{yy}(\omega)$. As is shown in *Fig. 2*, the proposed approach starts with m measured SLEs each one obtained from a cutting test with the same axial depth of cut a_p, radial depth of cut a_r and feed per tooth f_z but different spindle speeds w_i. Each SLE is moved to the frequency domain by performing an Inverse Fourier Transform obtaining SLE(ω). Along with the error spectrum for each w_i considered the cutting force spectrum $F_y(\omega)$ is computed from a lumped mechanistic model considering the cutting parameters, the tool geometry (i.e., tool diameter D, helix angle α_{el}, number of flutes N) the cutting coefficients (i.e., K_{tc} and K_{rc}) and the number of harmonics n.

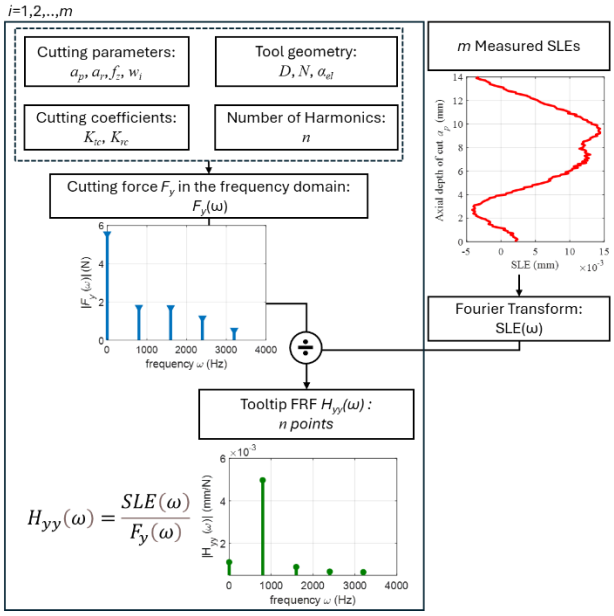

Fig. 2: Proposed approach: overview.

Finally, for each measurement available, the cutting force spectrum $F_y(\omega)$ and the error spectrum SLE(ω) are coupled in agreement with the n harmonics considered for the force spectrum to obtain n points of $H_{yy}(\omega)$ at different frequencies f_k according to the following equations:

$$f_k = kf_{tp} \quad k = 0,1,2,\ldots,n \tag{7}$$

$$f_{tp} = w_i N/60 \quad i = 1,2,\ldots,m \tag{8}$$

where f_{tp} is the tooth passing frequency for the i-th test. In this regard it must be noted that the tool considered for the proposed approach is simplified to be a constant pitch cutter with no runout. In the end, m x n points of $H_{yy}(\omega)$ are

found allowing for an accurate representation of the tooltip FRF. In the following sections details regarding the two main components of the proposed approach (i.e, the cutting force spectrum and the measured SLE) are presented.

2.1 Cutting force Spectrum

The first component of the proposed approach is the cutting force spectrum $F_y(\omega)$, which is computed following the model proposed by Morelli et al. [Morelli 2022] for an ideal endmill with constant pitch and no runout. In detail, the model expresses the cutting force F_y in time domain as Fourier series including the effect related to the helix angle without requiring any discretization. Following this model F_y is expressed as:

$$F_y(\phi) = a_0^* \cdot N a_p + \sum_{j=1}^{N} \sum_{v=1}^{n} \left(\left(\left(\frac{a_v^*}{v k_b} \sin v k_b a_p + \frac{b_v^*}{v k_b} \cos v k_b a_p - \frac{b_v^*}{v k_b} \right) \cos v \phi_j + \left(- \frac{a_v^*}{v k_b} \cos v k_b a_p + \frac{a_v^*}{v k_b} + \frac{b_v^*}{v k_b} \sin v k_b a_p \right) \sin v \phi_j \right) \right) \quad (9)$$

$$\phi_j = wt + \left(\frac{2\pi}{N} \right) (j-1) \quad j = 1,2,\dots,N \quad (10)$$

where t is the time variable, v is the index identifying the v-th harmonic considered for the frequency domain representation of F_y and a_0^*, a_n^* and b_n^* are the Fourier series coefficients which depend on the cutting coefficients (i.e., K_{tc} and K_{rc}), the radial depth of cut (a_r) and the feed per tooth (f_z). The full expression of the Fourier series coefficients is reported in Appendix A at the end of the paper.

2.2 Measured SLE

The other component of the proposed approach is represented by the measured SLEs. In detail, it is essential to ensure that the error spectrum SLE(ω) reflects at least one period of the cutting force $F_y(\omega)$ otherwise the frequency content of the two elements to couple is not the same. To satisfy this condition, the machined surface must be generated in an interval higher than the tooth passing period; From an analytical point of view this condition is expressed as:

$$\alpha_{sw} > \frac{2\pi}{N}; \quad (11)$$

Rearranging the terms of Eq.11 an expression for the axial depth of cut a_p to be satisfied during the cutting test is found:

$$a_p > \frac{2\pi}{N k_b}; \quad (12)$$

Eq.12 shows that the necessary axial depth of cut to perform a suitable cutting test for the SLE measurement depends only on the tool geometry, and it represents a limit of the proposed approach since not every tool geometry would allow a feasible axial depth of cut. Along with Eq.12, it is worth defining the axial depth of cut a_p^* corresponding to the tooth passing period:

$$a_p^* = \frac{2\pi}{N k_b}; \quad (13)$$

It must be noted that if the interval in which the machined surface is created and the tooth passing period are equal (i.e., a_p=a_p^*) the approach would fail since in such conditions the cut tends to be continuous and almost constant leading to a neglectable frequency content of the cutting force, therefore it is important that Eq.12 is satisfied.

Another aspect to highlight is that to obtain the error spectrum SLE(ω) in the frequency domain first the measured SLE needs to be moved from the spatial domain to the time domain, so the axial position z_e^s of the s-th point representing the surface error profile is rearranged in the time domain as:

$$t_e^q = \frac{z_e^q}{k_b 2\pi w} \quad q = 1,2,\dots,p \quad (14)$$

where t_e^q is the time instant in which the surface error point q at a position z_e^q is created during the cutting process, and p is the number of points defining the SLE profile.

3 EXPERIMENTAL VALIDATION

The proposed method has been experimentally tested to verify its effectiveness; Several milling tests were conducted in both down-milling and up-milling measuring the SLEs obtained.

3.1 Set-up

A DMG MORI DMU 75 machine-tool with an on-board measuring probe RENISHAW OMP 60 (*Fig. 3*a) was used for the measurement of the machined surface. Peripheral cutting milling tests were performed with a GARANT 202512M endmill with 218mm of overhang (*Fig. 3*b) on an Aluminum 6082 workpiece 75x120x40mm.

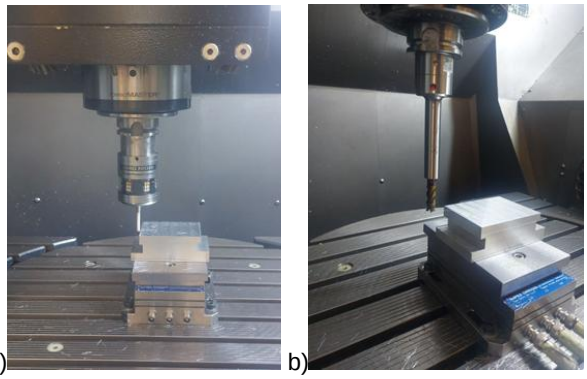

a) b)

Fig. 3: a) Measuring probe b) Endmill Garant 202512M.

The tool geometry and the fixed cutting parameters adopted are summarized in *Tab. 1.*

Tab. 1: Endmill geometry and fixed cutting parameters.

D(mm)	***α_{el}(deg)***	***N***	***a_p*(mm)**	**a_r(mm)**	***f_z*(mm)**
12	38	4	14	0.8	0.1

The axial depth of cut was selected in agreement with Eq.12, indeed for the endmill considered a_p must be higher than 12.08mm according to Eq.13. Instead, for the evaluation of cutting force spectrum $F_y(\omega)$ the parameters adopted are shown in *Tab. 2.*

Tab. 2: Cutting force spectrum $F_y(\omega)$ parameters.

K_{tc}(N/mm^2)	***K_{rc}(N/mm^2)***	***n***
609.84	162.40	5

Peripheral milling tests were conducted with five different spindle speeds so that a consistent range of frequencies was covered in the tooltip FRF evaluation. For each spindle speed, both down-milling and up-milling strategy were tested. A summary of all the frequencies analyzed is reported in *Tab. 3.*

Regarding the experimental SLEs, in each test 5 sets of error profile were measured with 0.1mm steps along the axial depth of cut to ensure a high frequency resolution in the error spectrum SLE(ω).

Tab. 3: Spindle speeds and frequencies investigated.

Test	w(rpm)	f_1(Hz)	f_2(Hz)	f_3(Hz))	f_4(Hz)
1	3500	233	466	700	933
2	6300	420	840	1260	1680
3	8500	566	1133	1700	2266
4	12000	800	1600	2400	3200
5	10200	680	1360	2040	2720

3.2 Tooltip FRF identification

The results obtained are presented in this section distinguishing down-milling and up-milling cases. In detail SLEs are shown in the spatial domain within the interval between 0 and a_p^* according to Eq.13 (i.e., a_p^*=12.08mm); In the frequency domain SLEs and cutting force $F_y(\omega)$ spectra are presented as amplitude spectrum. The tooltip FRF $H_{yy}(\omega)$ obtained with the proposed approach was compared with the one measured with the conventional Impact Hammer Testing method. In particular, the static stiffness k_y and the natural frequency f_n defining the tooltip FRF of the two methods were compared in terms of relative error e_r:

$$e_r = \frac{g_h - g_p}{g_h} \%; \quad (15)$$

Where g_h and g_p are the generic parameters defining the tool tip FRF (i.e. k_y and f_n) with the Impact Hammer Testing and the proposed approach respectively. The static stiffness and the natural frequency obtained from Impact Testing methods are reported in *Tab. 4*.

Tab. 4: Impact Hammer Testing tooltip FRF parameters.

k_y(mm/N)	f_n(Hz)
9.242e-04	680

Moreover, to check the whole evolution of the tooltip FRF the points of $H_{yy}(\omega)$ found and the FRF obtained from impact testing were compared in terms of Root Mean Squared Deviation (RMSD) with the following equation:

$$RMSD = \sqrt{\frac{\sum_1^{n_p}(x_h - x_p)^2}{n_p}}; \quad (16)$$

Where x_h and x_p are the points of the FRF found with Impact Testing and the proposed approach respectively, n_p is the number of points available.

Down-milling

Fig. 4 shows the experimental SLEs and their amplitude spectrum |SLE(ω)| for the five cutting tests. As the spindle speed changes, given the same cutting parameters, the SLE shape changes showing oscillations increasingly higher as the cutting force harmonics gets close to the natural frequency of the tool between 500Hz and 1000 Hz.

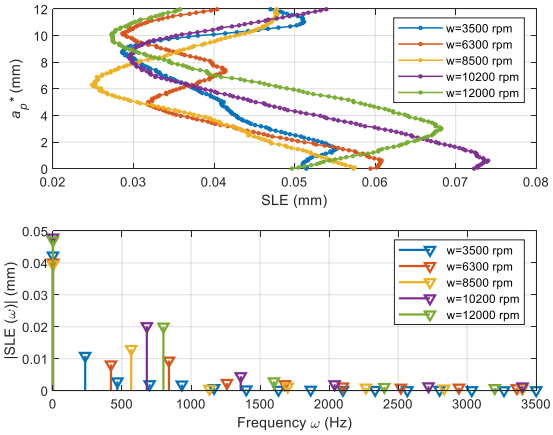

Fig. 4: SLEs analysis down-milling

Indeed, the amplitude of the error profiles varies from 0.013mm with 3500 rpm up to 0.023mm at 10200 rpm. Nonetheless the mean value of the SLE is almost constant over the five tests, ranging from 0.047mm to 0.04mm in agreement with the cutting force spectrum which presents the same mean value at 0 frequency. In this regard *Fig. 5* shows the amplitude cutting force spectrum $|F_y(\omega)|$ and the amplitude spectrum of the $H_{yy}(\omega)$ points found with the proposed approach for the five tests considered. In the cutting force spectrum, independently from the test analyzed, the amplitude of the harmonics does not change since the cutting parameters are the same in every test. Instead, the tooth passing frequency f_{tp} changes at every test so that the same harmonics excite different portions of the tool FRF.

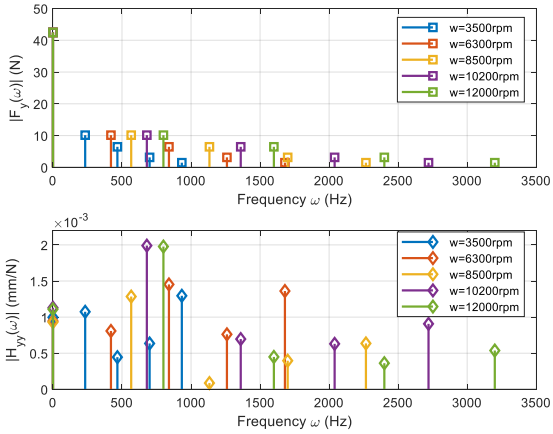

Fig. 5: $|F_y(\omega)|$ spectrum and $|H_{yy}(\omega)|$ spectrum down-milling.

The $H_{yy}(\omega)$ points found presents an evolution in agreement with a tooltip FRF with an almost constant value at 0 Hz ranges from 0.0093 to 0.011 mm/N representing the static stiffness k_y. Instead, the natural frequency was computed analyzing the evolution of the real part of the $H_{yy}(\omega)$ points obtaining a value of 488 Hz.

For a deeper comprehension of the results obtained the $H_{yy}(\omega)$ points found were ordered according to their frequency and compared with the tooltip FRF obtained with a conventional Impact Hammer Testing method. For this comparison, the mean value of the five harmonics at zero frequency was used as static stiffness value k_y. The comparison is shown in *Fig. 6* in terms of amplitude spectrum.

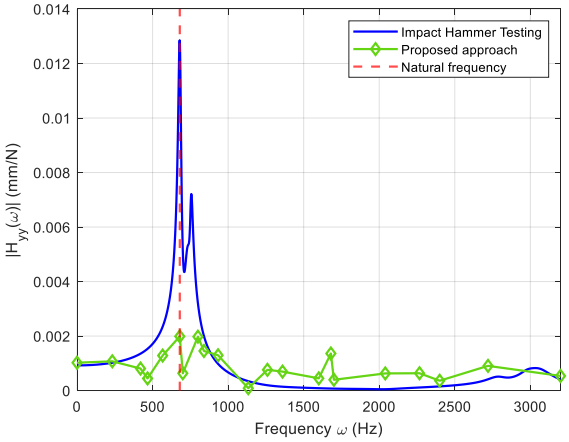

Fig. 6: Down-milling -Comparison $|H_{yy}(\omega)|$ - Impact Hammer Testing and Proposed approach

In this case the evolution of the points found fails to represent the overall tooltip FRF giving an RMSD of 0.0026 mm/N, yet the static stiffness is in line with the ones obtained from the testing with a relative error of 10% (k_{yp} =0.001 mm/N). Instead, the natural frequency obtained from the analysis of the real part of the $H_{yy}(\omega)$ points showed a significant deviation with a relative error of 28%.

Analyzing the tooltip FRF as a complex number in terms of real and imaginary part, the comparison between the proposed and the Impact Hammer testing is shown in *Fig. 7*; In this representation it can be seen how the proposed approach manages to evaluate correctly the tooltip static stiffness k_y, but it fails to reproduce the evolution of the FRF in the range where the natural frequency is found. However, beyond the range of the natural frequency despite the reduction in the amplitudes of both forces and SLEs the proposed method reproduced correctly the evolution of both real and imaginary parts of $H_{yy}(\omega)$.

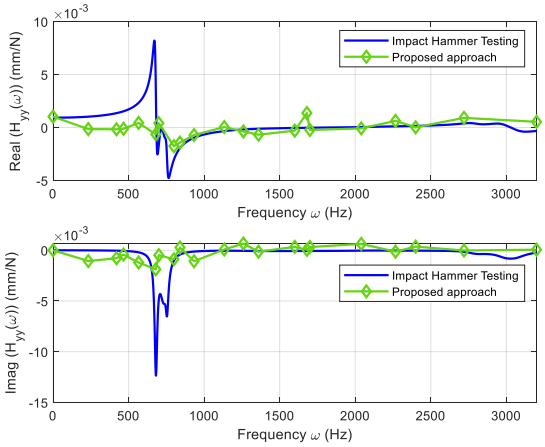

Fig. 7: Down-milling -Comparison real and imaginary part of $H_{yy}(\omega)$ - Impact Hammer Testing and Proposed approach

Up-milling

In up-milling, given the same cutting parameters (i.e., axial depth of cut a_p, radial depth of cut a_r, feed per tooth f_z and spindle speed w) the SLEs significantly change compared to down-milling, as it is shown in *Fig. 8*. In detail, both error shape and error magnitude reduce with amplitudes ranging from 0.007mm at 3500rpm to 0.019mm at 10200 rpm. Furthermore, in this case the mean value of the SLEs varies from 0.002mm to 0.01mm, and a clear peak between 500 Hz and 1000 Hz is found.

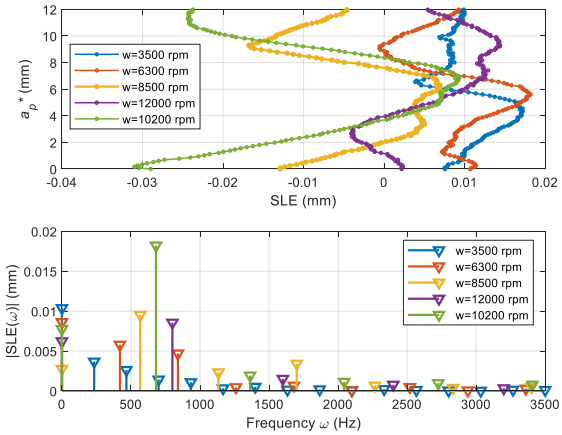

Fig. 8: SLEs analysis up-milling

The higher deviation in the mean value of SLEs is due to the reduced magnitude of the errors which makes random errors of the measurements more significant. In this regard the up-milling milling strategy is characterized by lower magnitude given the same cutting parameters compared to down-milling; Moreover, the cutting force profile in up-milling also changes resulting in different error shapes. These aspects are highlighted in *Fig. 9* where the amplitude spectrum of both cutting force $F_y(\omega)$ and the $H_{yy}(\omega)$ points for the up-milling strategy are shown.

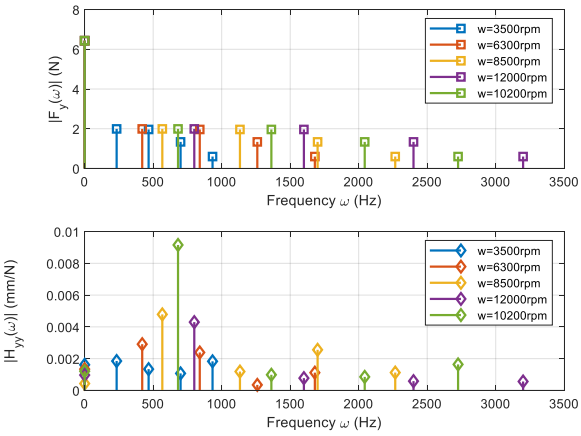

Fig. 9: $|F_y(\omega)|$ spectrum and $|H_{yy}(\omega)|$ spectrum up-milling.

Regarding the tooltip FRF, the $H_{yy}(\omega)$ points obtained in up-milling better represents the evolution of a conventional Tooltip FRF with a more defined peak and a static stiffness ranging from 0.0004 mm/N to 0.0016 mm/N. Instead, the natural frequency obtained by analyzing the evolution of the real part of the $H_{yy}(\omega)$ points was 741 Hz.

Comparing the $H_{yy}(\omega)$ points with the tooltip FRF obtained from Impact Hammer Testing method, as it is shown in *Fig. 10*, the results significantly differ from the down-milling case. Indeed, the proposed approach better represents the evolution of the tooltip FRF with a RMSD of 0.0016 mm/N and a static stiffness k_{yp} found from the mean of the five harmonics at zero frequency of $H_{yy}(\omega)$ of 0.0011 mm/N. In terms of relative error e_r, a value of 14% for static stiffness and 9% for the natural frequency were found; These results are acceptable considering the number of points available.

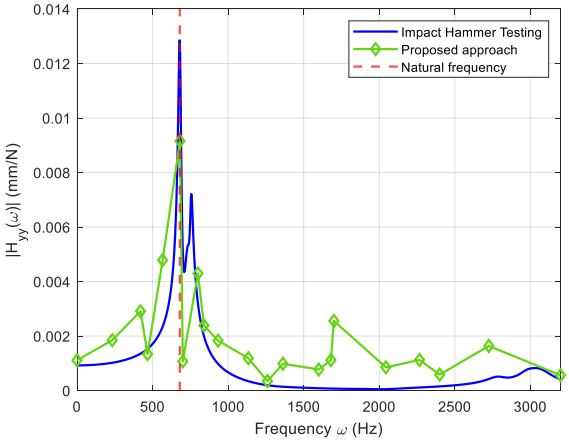

Fig. 10: Up-milling -Comparison $|H_{yy}(\omega)|$ - Impact Hammer Testing and Proposed approach

Analyzing the real and imaginary parts of the tooltip FRF an additional comparison between the proposed approach and the Impact Testing Method is reported in *Fig. 11.*

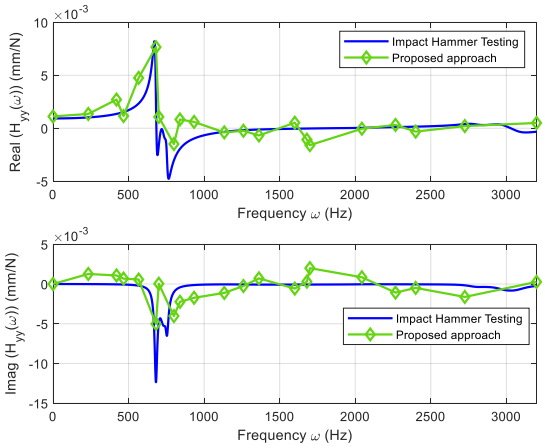

Fig. 11: Up-milling -Comparison real and imaginary part of $H_{yy}(\omega)$ - Impact Hammer Testing and Proposed approach

In agreement with the amplitude spectrum, with the up-milling strategy, the proposed approach better represents the evolution of the tooltip FRF even in the range of natural frequency between 500 Hz and 1000 Hz. Nonetheless, the peak of the tooltip FRF in terms of amplitude significantly differs in the two approaches considered. This discrepancy is probably related to the different operational conditions in which the tooltip FRF is measured. Furthermore, in the frequency range outside of the natural frequency (i.e., from 0 to 500 Hz and from 1000 to 3200 Hz) the proposed approach well manages to reproduce the evolution of the tooltip FRF in line with the down-milling strategy case.

3.3 Cutting strategy considerations

In the previous section the proposed approach was tested considering both down-milling and up-milling strategies. In both cases the proposed approach manages to indirectly measure the tooltip FRF in the frequency range outside the natural frequency, yet in the frequency range near the natural frequency the up-milling strategy performed significantly better than the down-milling one given the same cutting parameters. The reason for this difference is probably related to mechanisms which the SLE closed form proposed by Schmitz et al. [Schmitz and Mann 2006] do not account for and are more significant in down-milling compared to the up-milling strategy.

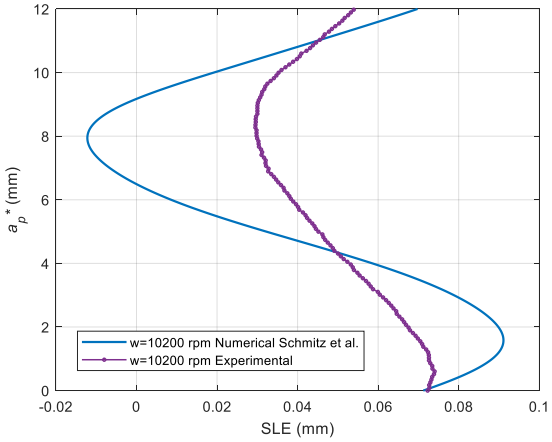

Fig. 12: Comparison between numerical and experimental SLE in Test 5 Down-milling

Indeed, referring to *Fig. 12* for Test 5, in down-milling, when the first harmonic of the cutting force excites the natural frequency of the tooltip (i.e., the tooth passing frequency matches the tooltip natural frequency) SLE is expected to be extremely high with an amplitude around 0.051mm according to the closed form solution, yet the experimentally measured SLE presents an amplitude of 0.023mm which is significantly lower. Nonetheless the shape of the measured SLE agrees with the one computed by the closed form.

In up-milling given the same conditions (i.e., the tooth passing frequency matches the tooltip natural frequency), as it is shown in *Fig. 13,* SLE is expected to be lower with an amplitude of 0.018mm according to the model by Schmitz et al, and the experimental SLE presents an amplitude of 0.02mm in line with the analytical model considered. Furthermore, the shape of the experimental SLE is analogous to the ones computed numerically.

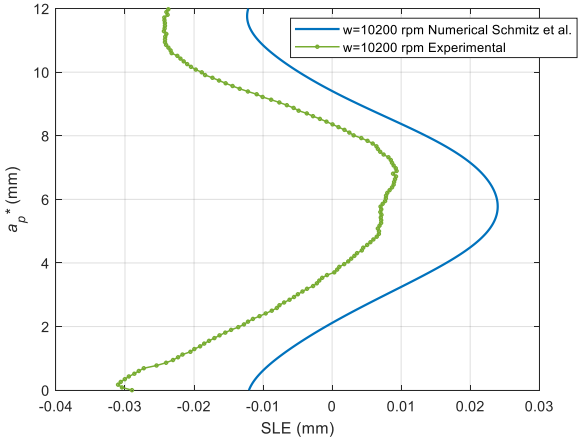

Fig. 13: Comparison between numerical and experimental SLE in Test 5 Up-milling

The only difference in the two cases is the cutting strategy which affects the cutting force F_y. Indeed, given the same cutting parameters in up-milling forces are lower causing minor vibrations even when the tooth passing frequency matches the natural frequency of the tool, while in down-milling the cutting force F_y is higher leading to higher vibrations. In this regard, vibrations affect the actual engagement conditions during the cut reducing the radial depth of cut a_r. This aspect could explain the huge deviations between numerical and experimental SLE in down-milling, since lower radial depths reduce the cutting

forces and the resulting SLEs. However, in down-milling, the reduction of the radial depth of cut is not enough to compensate for the deviation between numerical and experimental SLE suggesting that another mechanism is occurring when the tooth passing frequency is exciting the tooltip natural frequency. In the author's opinion, not only the vibration in cross-feed direction affects the actual engagement conditions, reducing the radial depth of cut a_r but also the vibration in the feed-direction impacts on the engagement conditions, reducing the feed per tooth f_z. This aspect together with the reduction of the radial depth of cut could explain the significant deviation in test 5 in down-milling, while for test 5 in up-milling, these aspects become less relevant due to the reduced vibrations which cause a minor reduction of radial depth of cut a_r and feed per tooth f_z.

4 CONCLUSIONS

In milling, vibrations are one of the main causes of inaccuracies and poor finishing. Most of the methods dealing with vibrations are based on the tooltip Frequency Response Function (FRF) which quantify how the tooltip response in terms of displacement to an excitation at different frequencies. Conventional methods to measure the tooltip FRF are usually expensive and time consuming since additional sensors must be mounted on the machine tool and operators with specific expertise are required due to the poor repeatability of the measurements.

This paper investigates a novel method to indirectly measure the tooltip FRF in peripheral milling without requiring any additional sensors to be mounted on the machine tool or any operator with specific expertise. In detail, the proposed approach exploits the on-board measuring probe to measure the Surface Location Errors (SLEs) in different cutting tests performed with the same cutting parameters (i.e., axial depth of cut a_p, radial depth of cut a_r and feed per tooth f_z) but different spindle speeds. These measurements are coupled with a cutting force model in the frequency domain for an ideal endmill with no constant pitch and no runout to invert the closed form for SLE and obtain an indirect evaluation of the tooltip FRF.

The proposed method was experimentally tested considering both down-milling and up-milling strategy. In both cases the method proved to be a satisfactory alternative for the evaluation of the tooltip static stiffness with a maximum relative error of 14% compared to the conventional Impact Hammer Testing Method, however for the tooltip FRF measurement, the up-milling strategy performed significantly better than down-milling with a relative error of 9% for the natural frequency and a reduced RMSD compared the down-milling.

The reasons for these differences are related to the simplicity of the analytical model adopted since additional mechanisms need to be included for a better tooltip FRF evaluation in down-milling. On the other hand, in up-milling, these mechanisms are less relevant due to the reduced cutting forces allowing for a better tooltip FRF measurement despite the simplicity of the analytical model adopted.

Overall, the proposed approach represents a promising alternative for the indirect measurement of the tooltip FRF considering only SLEs obtained from up-milling cutting tests. Future activities will focus on structuring the proposed approach in terms of SLE measurements and spindle speeds with the aim of reducing the time required for surface measurement. In this context, spindle speed ramp up technique could be an interesting fit for the proposed approach. Furthermore, the analytical model used as reference should be improved to account for the other mechanisms occurring in the surface generation with the aim of increasing the effectiveness of the proposed approach.

5 REFERENCES

[Aguirre 2014] Aguirre, G., et al. Real milling force based dynamic parameter extraction method, Proceedings of ISMA (2014).

[Iglesias 2022] Iglesias, A., et al. Alternative experimental methods for machine tool dynamics identification: A review. Mechanical Systems and Signal Processing, 2022, Vol.170 pp.108837. doi: 10.1016/J.YMSSP.2022.108837

[Kleinwort 2016] Kleinwort, R., et al. Comparison of Different Control Strategies for Active Damping of Heavy Duty Milling Operations, Procedia CIRP, 2016, Vol.46, pp. 396–399. doi: 10.1016/J.PROCIR.2016.04.054

[Kolluru 2013] Kolluru, K., Axinte, D. and Becker A. A solution for minimising vibrations in milling of thin walled casings by applying dampers to workpiece surface, CIRP Annals, 2013, Vol.62, No.1, pp.415–418. doi: 10.1016/J.CIRP.2013.03.136

[Llanos 2023] Llanos, I., et al. Deflection error modeling during thin-wall machining, Procedia CIRP, 2023, Vol.117, pp.169–174. doi: 10.1016/J.PROCIR.2023.03.030

[Mann 2008] Mann, B. P., et al. Chatter vibration and surface location error prediction for helical end mills, International Journal of Machine Tools and Manufacture, 2008, Vol.48, No.3–4, pp.350–361. doi: 10.1016/J.IJMACHTOOLS.2007.10.003

[Morelli 2022] Morelli, L., et al. Surface location error prediction in 2.5-axis peripheral milling considering tool dynamic stiffness variation, Precision Engineering, 2022, Vol.76, pp.95–109. doi: 10.1016/j.precisioneng.2022.03.008

[Morelli 2021] Morelli, L., et al. Extended classification of surface errors shapes in peripheral end-milling operations, Journal of Manufacturing Processes, 2021, Vol.71, pp 604–624. doi: 10.1016/j.jmapro.2021.09.054

[Munoa 2016] Munoa, J., et al. Chatter suppression techniques in metal cutting, CIRP Annals, 2016, Vol.65, No.2, pp.785–808. doi: 10.1016/j.cirp.2016.06.004

[Niu 2021] Niu, J., et al. State dependent regenerative stability and surface location error in peripheral milling of thin-walled parts. International Journal of Mechanical Sciences, 2021, Vol.196, pp.106294. doi: 10.1016/J.IJMECSCI.2021.106294

[Schmitz and Mann 2006] Schmitz, T. L. and Mann, B. P. Closed-form solutions for surface location error in milling, International Journal of Machine Tools and Manufacture, 2006, Vol.46, No.12, pp.1369–1377. doi: 10.1016/j.ijmachtools.2005.10.007

[Tunc and Budak 2013] Tunc, L. T. and Budak, E. Identification and modeling of process damping in milling, Journal of Manufacturing Science and Engineering, 2013, Vol.135, No.2. doi: 10.1115/1.4023708/375042

[Wiederkehr 2020] Wiederkehr, P., Wilck, I. and Siebrecht, T. Determination of the dynamic behaviour of micro-milling tools at higher spindle speeds using ball-shooting tests for the application in process simulations, CIRP Annals, 2020, Vol.69, No.1, pp.97–100. doi: 10.1016/J.CIRP.2020.04.036

[Zaghbani and Songmene 2009] Zaghbani, I.and Songmene, V. Estimation of machine-tool dynamic

parameters during machining operation through operational modal analysis, International Journal of Machine Tools and Manufacture, 2009, Vol.49, No.12–13, pp 947–957. doi: 10.1016/J.IJMACHTOOLS.2009.06.010.

APPENDIX A

The coefficients for the Fourier series computation of cutting forces are provided here.

Cutting force in cross-feed (y) considering edge coefficients

$$a_{y0}^{*} = -\frac{1}{2\pi}[K_{tc}f_z\left(-\frac{x}{2}+\frac{1}{4}\sin(2x)\right) - K_{rc}f_z\left(\frac{1}{4}\cos(2x)\right) + K_{te}\cos(x) + K_{re}\sin(x)]_{\phi_{in}}^{\phi_{out}} \quad (17)$$

$$a_{y1}^{*} = -\frac{1}{\pi}[K_{tc}f_z\left(-\frac{1}{4}\sin(x)+\frac{1}{12}\sin(3x)\right) + K_{rc}f_z\left(-\frac{1}{4}\cos(x)-\frac{1}{12}\cos(3x)\right) + K_{te}(\frac{1}{4}\cos(2x)) + K_{re}(\frac{1}{2}x+\frac{1}{4}\sin(2x)]_{\phi_{in}}^{\phi_{out}} \quad (18)$$

$$a_{y2}^{*} = -\frac{1}{\pi}[K_{tc}f_z\left(\frac{1}{4}x-\frac{1}{4}\sin(2x)+\frac{1}{16}\sin(4x)\right) - K_{rc}f_z\left(\frac{1}{16}\cos(4x)\right) + K_{te}(-\frac{1}{2}\cos(x)+\frac{1}{6}\cos(3x)) + K_{re}(\frac{1}{2}\sin(x)+\frac{1}{6}\sin(3x)]_{\phi_{in}}^{\phi_{out}} \quad (19)$$

$$a_{yj}^{*} = -\frac{1}{\pi}[K_{tc}f_z\left(-\frac{1}{2j}\sin(jx)+\frac{1}{4(j-2)}\sin\big((j-2)x\big)+\frac{1}{4(j+2)}\sin\big((j+2)x\big)\right) + K_{rc}f_z\left(\frac{1}{4(j-2)}\cos\big((j-2)x\big)-\frac{1}{4(j+2)}\cos\big((j+2)x\big)\right) + K_{te}(-\frac{1}{2(j-1)}\cos\big((j-1)x\big)+\frac{1}{2(j+1)}\cos\big((j+1)x\big)) + K_{re}(\frac{1}{2(j-1)}\sin\big((j-1)x\big)+\frac{1}{2(j+1)}\sin\big((j+1)x\big)]_{\phi_{in}}^{\phi_{out}} \quad (20)$$

$$b_{y1}^{*} = -\frac{1}{\pi}[K_{tc}f_z\left(\frac{3}{4}\cos(x)-\frac{1}{12}\cos(3x)\right) + K_{rc}f_z\left(\frac{1}{4}\sin(x)-\frac{1}{12}\sin(3x)\right) + K_{te}(-\frac{1}{2}x+\frac{1}{4}\sin(2x)) + K_{re}(-\frac{1}{4}\cos(2x)]_{\phi_{in}}^{\phi_{out}} \quad (21)$$

$$b_{y2}^{*} = -\frac{1}{\pi}[K_{tc}f_z\left(\frac{1}{4}\cos(2x)-\frac{1}{16}\cos(4x)\right) + K_{rc}f_z\left(\frac{1}{4}x-\frac{1}{16}\sin(4x)\right) + K_{te}(-\frac{1}{2}\sin(x)+\frac{1}{6}\sin(3x)) + K_{re}(-\frac{1}{2}\cos(x)-\frac{1}{6}\cos(3x)]_{\phi_{in}}^{\phi_{out}} \quad (22)$$

$$b_{yj}^{*} = -\frac{1}{\pi}[K_{tc}f_z\left(\frac{1}{2j}\cos(jx)-\frac{1}{4(j-2)}\cos\big((j-2)x\big)-\frac{1}{4(j+2)}\cos\big((j+2)x\big)\right) + K_{rc}f_z\left(\frac{1}{4(j-2)}\sin\big((j-2)x\big)-\frac{1}{4(j+2)}\sin\big((j+2)x\big)\right) + K_{te}(-\frac{1}{2(j-1)}\sin\big((j-1)x\big)+\frac{1}{2(j+1)}\sin\big((j+1)x\big)) + K_{re}(-\frac{1}{2(j-1)}\cos\big((j-1)x\big)-\frac{1}{2(j+1)}\cos\big((j+1)x\big)]_{\phi_{in}}^{\phi_{out}} \quad (23)$$